

Gyroscopic motion of superfluid trapped atomic condensates

Halvor Møll Nilsen [†], Dermot McPeake ^{‡*} and J F McCann [‡]

[†] Institute of Physics, University of Bergen, Allégaten 55, N-5007 Bergen, Norway

[‡] Dept of Applied Mathematics and Theoretical Physics, Queen's University Belfast, Belfast, BT7 1NN, Northern Ireland

* NMRC, University College Cork, Lee Maltings, Prospect Row, Cork, Ireland.

Abstract.

The gyroscopic motion of a trapped Bose gas containing a vortex is studied. We model the system as a classical top, as a superposition of coherent hydrodynamic states, by solution of the Bogoliubov equations, and by integration of the time-dependent Gross-Pitaevskii equation. The frequency spectrum of Bogoliubov excitations, including quantum frequency shifts, is calculated and the quantal precession frequency is found to be consistent with experimental results, though a small discrepancy exists. The superfluid precession is found to be well described by the classical and hydrodynamic models. However the frequency shifts and helical oscillations associated with vortex bending and twisting require a quantal treatment. In gyroscopic precession, the vortex excitation modes $m = \pm 1$ are the dominant features giving a vortex kink or bend, while the $m = +2$ is found to be the dominant Kelvin wave associated with vortex twisting.

1. Introduction

Superfluidity is one of the most dramatic illustrations of the quantum nature of matter. It is exemplified in its purest form in Bose-Einstein condensation [1] of cold atomic gases. The quantisation of angular momentum associated with the phase of the quantum fluid has been established through the nucleation of vortices [2, 3] recently extending to the observation of large vortex lattice structures with grain boundaries [4]. Experiments have also revealed collective irrotational oscillatory flows in the superfluid phase [5, 6] that revert to thermal flow modes and frequencies above the critical temperature.

One of the fundamental properties of a pure quantum fluid is the coherence of the phase of the wavefunction [7] where different regions of the condensate are phase-locked in their motion. For example, in the flow of an condensate past an obstacle, the requirement of upstream and downstream continuity in mass transport and phase gradient explains the capacity for superfluid flow [8], and the transition to dissipation when local phase slip arises. For homogeneous and inhomogeneous condensates, there is conclusive evidence, both theoretical and experimental, that the nucleation of vortices is the primary mechanism responsible for the onset of drag and dissipation in condensate flow [8, 9, 10]. Phase coherence is responsible for the quantisation of circulation (angular momentum) and the capacity of the fluid to conserve its state of rotation unless acted upon by a critical external moment. Consequently, it was predicted [11, 12] that a Bose-condensed gas could be made to exhibit gyroscopic motion. Very recently this phenomenon has been observed experimentally [13] and measured for the first time. In analogy with a spinning top, slightly displaced from equilibrium by an impulsive moment, a slight tilt of the axis of rotation (figure 1) produces precessional and nutational motion. In this paper we show that internal flows past the vortex create a Magnus force which results in precession, and that this combined with the inhomogeneity in the condensate gives rise to vortex bending and twisting into helical modes of oscillation.

The quantum gyroscope is also a unique diagnostic tool able to probe condensate flow velocities, acoustic waves, and pressures. The oscillating and twisting motion of a vortex, as we will show, is highly sensitive to density fluctuations and inhomogeneities. In this paper we study the dynamics of a single-quantum vortex lying near the axis of a cylindrically symmetric trap. In our study we have employed four different methods of analysing the motion: (a) the Bogoliubov-de Gennes equations (b) the Gross-Pitaevskii equation, (c) hydrodynamic equations, and (d) classical equations. While methods (a) and (c) are essentially linearisations of (b), they are extremely important in identifying the underlying modes of excitation. We study the collective modes of the system and compare with recent hydrodynamic theory. We find that while many features of the gyroscopic motion are described by the hydrodynamic model, the vortex motion is significantly different. Firstly, the frequencies of precessional motion are shifted from the hydrodynamic predictions, secondly the vortex core has a single kink, and thirdly the vortex performs a helical Kelvin wave oscillation of mode $m = +2$ not previously seen.

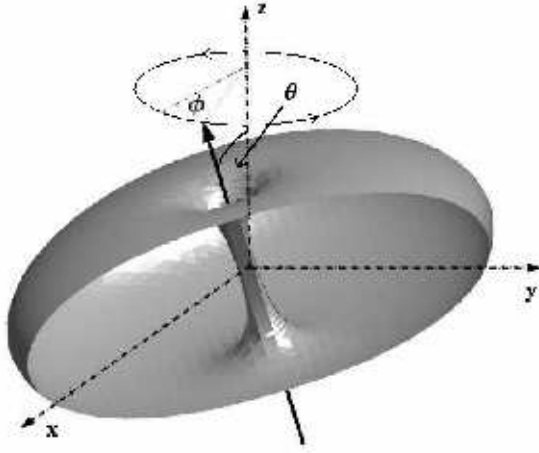


Figure 1. Classical rigid gyroscopic motion of the inhomogeneous trapped condensate. The figure indicates a surface of constant density for a singly-quantised gyroscope ($\kappa = 1$) corresponding to the ground state solution of the Gross-Pitaevskii equation with atom interaction strength $C = 1000$. The classical Euler angles [14], θ and ϕ , defining the orientation of the vortex are shown.

2. Formulation of the problem

For a cold weakly-interacting gas, the ground state (condensate mode) dominates the collective dynamics of the system. In experimental realizations one can achieve temperatures such that $T \ll T_c$ (typically 0.1 to 1 μ K) and densities such that the gas is weakly interacting and highly dilute. Under such conditions, the condensate of $N_0 \gg 1$ atoms is well described by a mean field, or wavefunction, governed by the Gross-Pitaevskii equation, and the quasiparticle excitations are acoustic waves within this field. If the perturbations of the condensate are small, then it is appropriate and convenient to use the linear response approximation, which is equivalent to the Bogoliubov approximation for single-particle excitations in highly-condensed quantised Bose gases at zero temperature.

Consider a dilute system of N_0 atoms, each of mass m_a , trapped by an external potential $V_{\text{ext}}(\mathbf{x}, t)$ and interacting weakly through the two-body potential $V(\mathbf{x}, \mathbf{x}')$. At low temperatures and densities, the atom-atom interaction can be represented perturbatively by the s -wave pseudopotential: $V(\mathbf{x}, \mathbf{x}') = (4\pi\hbar^2 a_s / m_a) \delta^{(3)}(\mathbf{x} - \mathbf{x}')$, and a_s is the s -wave scattering length. The dynamics follow from the Hartree variational principle:

$$\delta \int_{t_1}^{t_2} dt \int d^3\mathbf{x} \, \psi^* [H_0 + \frac{1}{2}g\psi^*\psi - i\hbar\partial_t] \psi = 0 \quad (1)$$

where $g = (4\pi\hbar^2/m_a)N_0a_s$, $H_0 = -(\hbar^2/2m_a)\nabla^2 + V_{\text{ext}} - \mu$, and the chemical potential μ plays the role of a Lagrange multiplier. The condensate and its excitations can be described

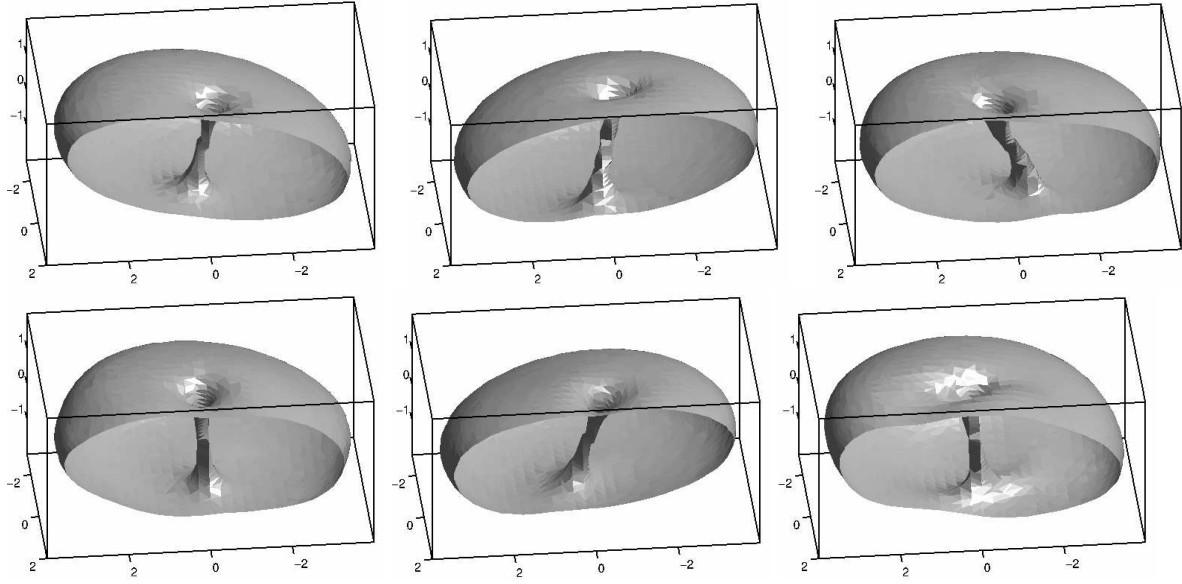


Figure 2. Surfaces of constant density of the condensate. Results from the solution of the Gross-Pitaevskii equation showing vortex bending and twisting, and condensate quadrupole oscillations in the scissors mode. A vertical cut through the surface reveals the vortex core shape. The images correspond to the parameters $C = 1000$, $\lambda = \sqrt{7}$, and angle $\theta_0 = 10^\circ$. The figure shows a sequence of frames at regular intervals. Top row, left to right $t = 0.0, 1.3, 2.6$, then bottom row, left to right $t = 3.9, 5.2$ and $t = 6.5$ in units of ω_0^{-1} . The vertical z -axis points in the direction of the axisymmetric trap axis. The unit of length on the figures is $(\hbar/2m_a\omega_0)^{1/2}$.

by the linear response ansatz:

$$\psi(\mathbf{x}, t) = a_0(t)\phi(\mathbf{x}) + \sum_{j>0} [a_j(t)u_j(\mathbf{x})e^{-i\omega_j t} + a_j^*(t)v_j^*(\mathbf{x})e^{+i\omega_j t}] \quad (2)$$

where ϕ represents the highly-occupied condensate; that is, $|a_0| \approx \sqrt{N} \gg |a_j|$, $j > 0$. From the variation $\delta\phi^*$, and linear expansion in the small parameters a_j, a_j^* taken as constant, the stationary Gross-Pitaevskii equation and Bogoliubov equations follow:

$$H_0\phi + g|\phi|^2\phi = 0 \quad (3)$$

with $(\phi, \phi) = 1$ and $\int d^3\mathbf{x} f(\mathbf{x})^*g(\mathbf{x}) \equiv (f, g)$. The Bogoliubov modes are solutions of the coupled linear equations:

$$(H_0 + 2g|\phi|^2)u_j + g\phi^2 v_j = +\hbar\omega_j u_j \quad (4)$$

$$(H_0 + 2g|\phi|^2)v_j + g\phi^{*2}u_j = -\hbar\omega_j v_j \quad (5)$$

Time-reversal symmetry of equations (4,5) is reflected in the fact that every set of solutions $\{\omega_j, u_j, v_j\}$ has a corresponding set $\{-\omega_j, v_j^*, u_j^*\}$ and the normalisation can be chosen conveniently, such that: $(u_i, u_j) - (v_i, v_j) = \delta_{ij}$.

2.1. Superfluid dynamics

The equivalent fluid motion is expressed through the coupled differential equations for mass and momentum transport [8]. The mass density ρ and momentum current density \mathbf{J} are

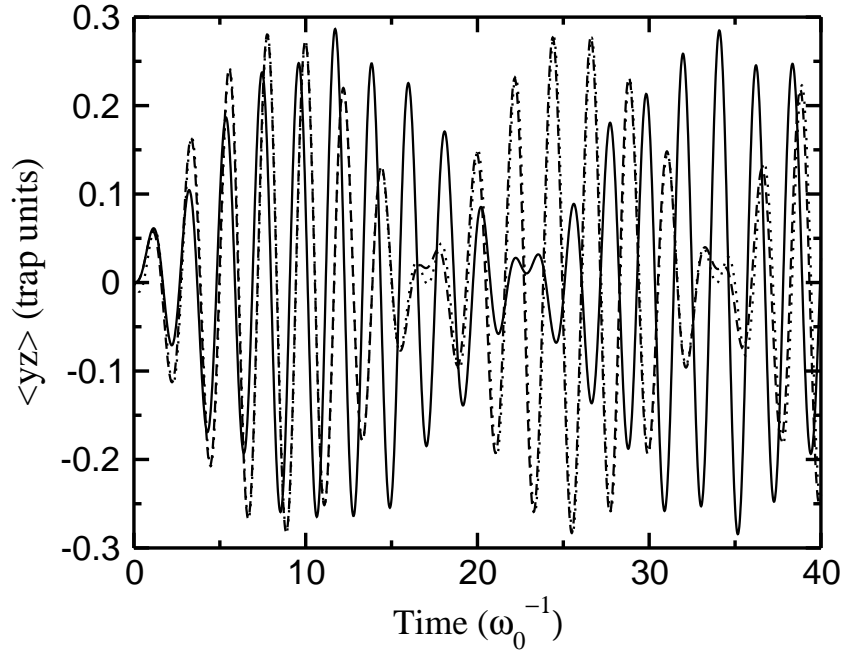


Figure 3. Quadrupole oscillations in the vertical plane. Results for $\langle yz \rangle(t) \equiv (2/N_0)Q_{yz}(t)$ for $\theta_0 = 4^\circ$, $C = 1000$ and $\lambda = \sqrt{7}$ are shown. Gross-Pitaevskii simulation (solid line), coherent hydrodynamic state model (dotted line), and the classical model (dashed line). The quantum frequency shift leads to a slower precessional motion than predicted by classical theory.

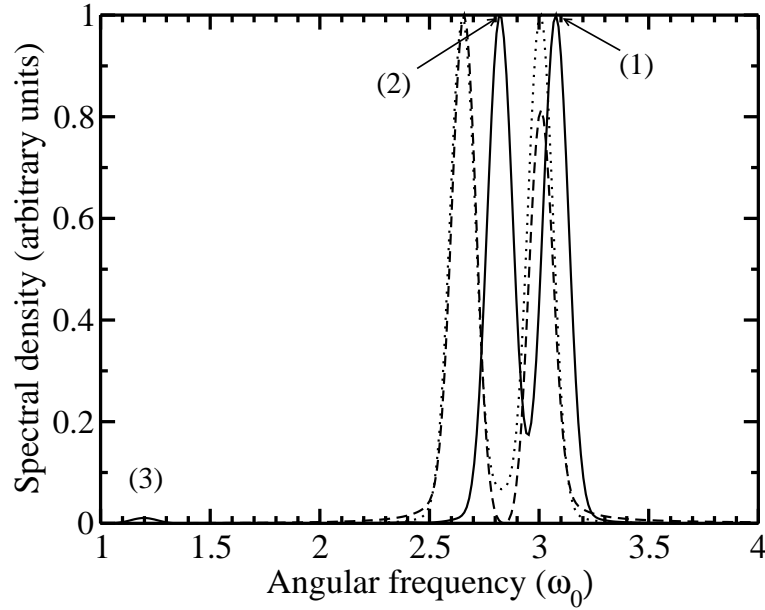


Figure 4. Spectral analysis $P_{yz}(\omega)$ (equation 29) of the vertical-plane quadrupole $\langle yz \rangle(t)$ shown in figure 3. The parameters are $\theta_0 = 4^\circ$, $C = 1000$, $\lambda = \sqrt{7}$. Results of Gross-Pitaevskii simulation (solid line) from equation (28), coherent hydrodynamic states (dotted line) from equation (39). Also shown is the classical model data (dashed line) obtained from equations (29) and (53). The higher frequency peak (1) corresponds to the quadrupole $(h; 0, 1, 1)/(i; 0, 2, 1)$ and the lower frequency (2) to the quadrupole $(h; 1, -1, 1)/(i; 1, 0, 1)$.

defined as, $\rho \equiv m_a \psi^* \psi$ and $J_k \equiv (\hbar/2i)(\psi^* \partial_k \psi - \psi \partial_k \psi^*)$, where the index k denotes the k th vector component, and repeated index summation convention is used. The fluid velocity is defined by $v_k \equiv J_k/\rho$, or equivalently in terms of the phase, χ , of the wavefunction, $v_k \equiv (\hbar/m_a) \partial_k \chi$. Then mass and momentum conservation are expressed by:

$$\partial_t \rho + \partial_j J_j = 0 \quad (6)$$

$$\partial_t J_k + \partial_j T_{jk} + \rho \partial_k (V_{\text{ext}}/m_a) = 0, \quad (7)$$

where the momentum flux density tensor is defined;

$$T_{jk} = \rho v_j v_k + \frac{1}{2} \delta_{jk} g (\rho/m_a)^2 - (\hbar/2m_a)^2 \rho \partial_j \partial_k \ln \rho. \quad (8)$$

Finally, the mass and momentum equations (6,7) combine to give the acoustic equation:

$$\partial_{tt} \rho = \partial_i \partial_j T_{ij} + \partial_i [\rho \partial_i (V_{\text{ext}}/m_a)] \quad (9)$$

The pressure is defined as [8], $p \equiv \frac{1}{2} g (\rho/m_a)^2 - (\hbar/2m_a)^2 \rho \nabla^2 \ln \rho$. The first term represents classical pressure, the second term is the quantum pressure and is discarded in the classical (hydrodynamic) approximation. The static ($J_k = 0$) equilibrium density in the hydrodynamic limit follows from (7):

$$\rho_0^{(h)}(\mathbf{x}) = (m_a/g) [\mu - V_{\text{ext}}(\mathbf{x}, 0)] \quad (10)$$

For small flow and density fluctuations about equilibrium, the kinetic energy and quantum pressure terms are small, so that: $T_{ij}^{(h)} \approx \frac{1}{2} g (\rho/m_a)^2 \delta_{ij}$. Using equation (9) the hydrodynamic acoustic modes given by $\rho(\mathbf{x}, t) = \rho_0^{(h)}(\mathbf{x}) + \bar{\rho}^{(h)}(\mathbf{x}) e^{-i\omega t}$ satisfy the linear eigenvalue problem:

$$-m_a \omega^2 \bar{\rho}^{(h)} = \partial_i [[\mu - V_{\text{ext}}(\mathbf{r}, 0)] \partial_i \bar{\rho}^{(h)}] \quad (11)$$

Finally, the relation of the torque (τ_i) by an external moment to the rate of change of angular momentum is given by:

$$\tau_i(t) = \partial_t \int_{\Omega} \epsilon_{ijk} x_j J_k d\Omega = - \int_{\Omega} \epsilon_{ijk} x_j [\partial_t T_{lk} + \rho \partial_k (V/m_a)] d\Omega \quad (12)$$

where the fluid occupies the volume Ω , and ϵ_{ijk} is the Levi-Civita symbol. Since $T_{ij} = T_{ji}$ it follows that:

$$\tau_i(t) = - \int_{\Omega} \epsilon_{ijk} \rho x_j \partial_k (V/m_a) d\Omega \quad (13)$$

The conservation of circulation, Kelvin's theorem, and its quantisation means that within the fluid, only those moments above a critical value can transfer angular momentum associated with vortex creation or destruction. Suppose the trap orientation changes with time, then the ellipsoidal potential can be written as the quadratic form: $V(t) = \frac{1}{2} a_{ij}(t) x_i x_j$ where $a_{ij} = a_{ji}$. Then the equation for superfluid motion, that is the absence of torque $\tau_i = 0$, is simply a set of homogeneous linear equations for the quadrupole moments of the condensate:

$$a_{kl}(t) \epsilon_{ijk} \int_{\Omega} \rho(\mathbf{x}, t) x_j x_l d\Omega = 0 \quad (14)$$

These moments are the key physical parameters for the condensate motion.

3. Methods

3.1. Bogoliubov-de Gennes equations

Consider the atoms confined by an oblate spheroidal (pancake-shaped) trap: $V_{\text{ext}}(\mathbf{x}, 0) = \frac{1}{2}m_a\omega_0^2(r^2 + \lambda^2 z^2)$, where r is the radial coordinate and z the axial coordinate, with $\lambda > 1$ the aspect ratio of the trap. For convenience we use scaled dimensionless units for length, time and energy namely: $(\hbar/2m_a\omega_0)^{\frac{1}{2}}$, ω_0^{-1} and $\hbar\omega_0$, respectively. We define the interaction strength by the dimensionless parameter $C \equiv 8\pi N_0 a_s (\hbar/2m_a\omega_0)^{-\frac{1}{2}}$, so that $C \rightarrow 0$ represents the ideal gas and $C \rightarrow \infty$, describes the hydrodynamic limit. Experiments studying the scissors and gyroscope modes performed by the Oxford group [15, 16, 17, 13] employ the atom Rb⁸⁷ for which $a_s \approx 110$ a.u.. So a typical value of C corresponding to a trap frequency $\omega_0 = 2\pi \times 110$ Hz and particle number $N_0 \sim 5000$ would be $C \sim 1000$, while $\omega_0 = 2\pi \times 62$ Hz with $N_0 \sim 19000$ is equivalent to $C \sim 2870$. In the ideal gas limit, the energy of the state which we label $(i; n_r, n_\theta, n_z)$, has the value:

$$E(i; n_r, n_\theta, n_z) = 2n_r + |n_\theta| + 1 + (n_z + \frac{1}{2})\lambda \quad (15)$$

with $n_\theta = 0, \pm 1, \pm 2, \dots$ and the radial and axial quantum numbers are: $n_r, n_z = 0, 1, \dots$. The corresponding excitation frequencies, with respect to a vortex state $(i; 0, \kappa, 0)$, where $\kappa = 0, \pm 1, \pm 2, \dots$, are given by:

$$\omega(i; n_r, n_\theta, n_z) = 2n_r + |n_\theta| - |\kappa| + n_z\lambda \quad (16)$$

For finite C , the spectrum of excitations must be determined by numerical solution of equations (3,4) and (5). Separating variables gives:

$$\phi(r, z, \varphi) = \tilde{\phi}_\kappa(r, z)e^{i\kappa\varphi} \quad (17)$$

so that the condensate with circulation κ is the solution of the equation:

$$-\left(\frac{\partial^2}{\partial r^2} + \frac{1}{r}\frac{\partial}{\partial r} + \frac{\partial^2}{\partial z^2} - \frac{\kappa^2}{r^2}\right)\tilde{\phi}_\kappa + \frac{1}{4}(r^2 + \lambda^2 z^2)\tilde{\phi}_\kappa + C|\tilde{\phi}_\kappa|^2\tilde{\phi}_\kappa = \mu\tilde{\phi}_\kappa \quad (18)$$

We use $m = n_\theta - \kappa$ to denote angular momentum with respect to the condensate, that is the helicity of the excitations, and it is convenient to use the labelling $(h; q_r, m, q_z)$ appropriate for the hydrodynamic limit ($C \rightarrow \infty$). Thus the quasiparticle amplitudes:

$$u_{n_r, m, n_z}(r, z, \varphi) \equiv \tilde{u}_{n_r, n_z}(r, z)e^{i(m+\kappa)\varphi} \quad \text{and} \quad v_{n_r, m, n_z}(r, z, \varphi) \equiv \tilde{v}_{n_r, n_z}(r, z)e^{i(m-\kappa)\varphi} \quad (19)$$

with corresponding angular frequency, ω_{n_r, m, n_z} , are solutions of the eigenvalue problem

$$\mathcal{L}(m + \kappa)\tilde{u}_{n_r, n_z}(r, z) + C\tilde{\phi}_\kappa^2\tilde{v}_{n_r, n_z}(r, z) = \omega_{n_r, m, n_z}\tilde{u}_{n_r, n_z}(r, z) \quad (20)$$

$$\mathcal{L}(m - \kappa)\tilde{v}_{n_r, n_z}(r, z) + C\tilde{\phi}_\kappa^{*2}\tilde{u}_{n_r, n_z}(r, z) = \omega_{n_r, m, n_z}\tilde{v}_{n_r, n_z}(r, z) \quad (21)$$

where

$$\mathcal{L}(s) \equiv -\left(\frac{\partial^2}{\partial r^2} + \frac{1}{r}\frac{\partial}{\partial r} + \frac{\partial^2}{\partial z^2} - \frac{s^2}{r^2}\right)\tilde{\phi}_\kappa + \frac{1}{4}(r^2 + \lambda^2 z^2)\tilde{\phi}_\kappa + 2C|\tilde{\phi}_\kappa|^2 \quad (22)$$

In our calculations, these two-dimensional equations are discretised by Lagrange meshes [18]; the radial coordinate is defined at M grid points (r_1, r_2, \dots, r_M) and the axial coordinate at N points (z_1, z_2, \dots, z_N) . Therefore:

$$\tilde{\phi}_\kappa(r, z) = \sum_{k=1}^M \sum_{l=1}^N \tilde{\phi}_\kappa^{kl}(r_k, z_l) \lambda_k^{-1/2} \mu_l^{-1/2} f_k(r) g_l(z) \quad (23)$$

where f, g are Lagrangian interpolating functions such that

$$\int_0^\infty f_i^*(r) f_k(r) 2\pi r dr \approx \lambda_i \delta_{ik} \quad (24)$$

$$\int_{-\infty}^\infty g_j^*(z) g_l(z) dz \approx \mu_j \delta_{jl} \quad (25)$$

The Lagrange functions for the r -coordinate are chosen to be generalised Laguerre polynomials [18], scaled to encompass the entire condensate, with typically $M = 50$ mesh points. Hermite polynomials are used in the z -direction so that

$$g_l(z) = \sum_{l=0}^{N-1} \chi_l^*(z_l) \chi_l(z) \quad (26)$$

where $\chi_l(z) = h_N^{-\frac{1}{2}} w(z)^{\frac{1}{2}} H_l(z)$. and $H_l(z)$ are the Hermite polynomials associated with weights $w(z) = e^{-z^2}$ and normalisation factor $h_N = 2^N \pi^{1/2} N$. A high degree of accuracy was found with only $N = 30$ points. The resultant eigenvalue problem was solved using Newton's method for equation (18) and a standard eigenvalue routine for equations (20,21). Convergence was established by a combination of grid scaling and number of mesh points, so that at least six-figure accuracy was assured for all frequencies (see table 1).

3.2. Time-dependent Gross-Pitaevskii equation

The time-dependent Gross-Pitaevskii equation, follows from taking arbitrary variation of ψ^* in (1):

$$[H_0 + g|\psi|^2 - i\hbar\partial_t] \psi = 0 \quad (27)$$

The direct numerical solution of this equation, without linearisation, in combination with spectral analysis can also be used to determine the frequency spectrum [18] and density fluctuations of the collective excitations. This can be done efficiently and accurately using spectral methods. The ground state of the system is found by evolving equation (27) in imaginary time using the split-step Fast-Fourier transform propagator [18]. A simple arbitrary trial function is used as the initial state. At each time step in the evolution the fluid circulation is imposed by applying a phase gradient corresponding to $\kappa = +1$ until the excited states diffuse from the system and the density and chemical potential stabilise. In practice this normally takes a few trap periods at most. Having found the condensate in this manner, the system is then allowed to evolve in real time under any external perturbations using the same numerical method.

For example a sudden rotation of the trap by a small angle will disturb the steady state flow of the condensate and create a variety of small amplitude excitations. Under these

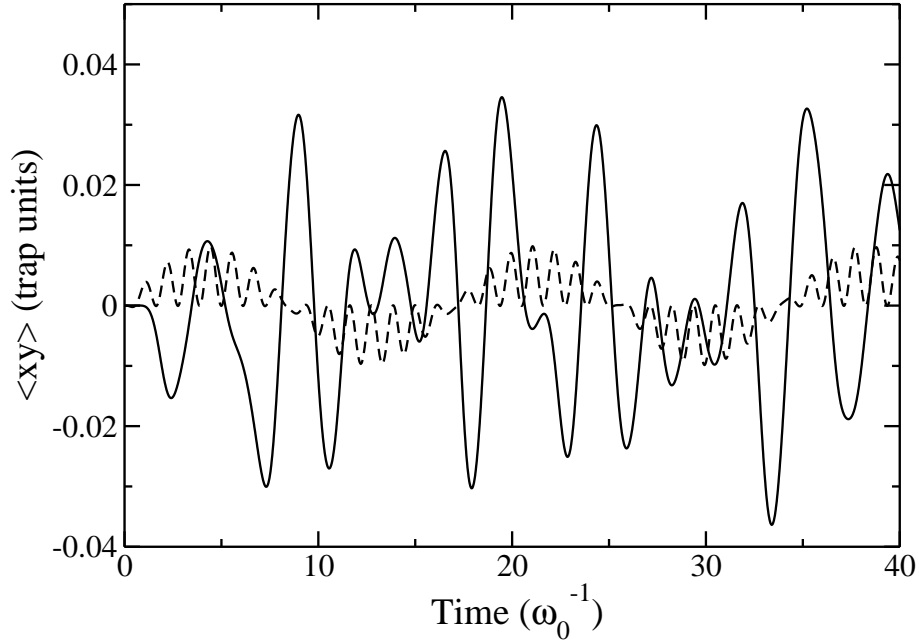


Figure 5. Quadrupole variations in the horizontal plane. Results for $\langle xy \rangle(t) \equiv (2/N_0)Q_{xy}(t)$ for angle $\theta_0 = 4^\circ$, $C = 1000$ and $\lambda = \sqrt{7}$. The full line is the Gross-Pitaevskii quantal simulation, the dashed line is the classical model. In contrast to the results in figure 3, the two models strongly disagree.

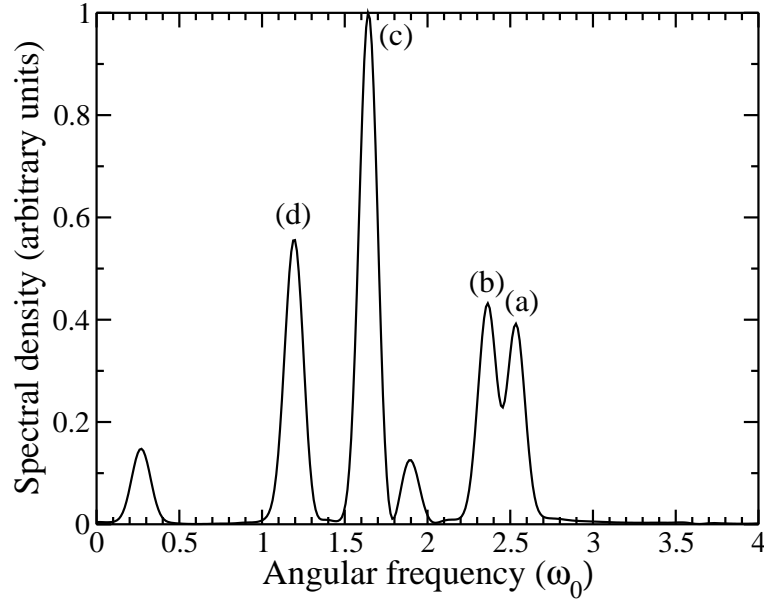


Figure 6. Helical mode spectrum: the power spectrum $P_{xy}(\omega)$, given by equation (29) of the horizontal-plane quadrupole shown in figure 5. The Kelvin mode, (c) $m = +2$, is most strongly excited and leads to helical oscillations of the vortex core. The mode (d) $m = -2$ is more weakly coupled, and the lines (a,b) associated with $m = \pm 1$ approximately cancel.

conditions, the linearisation (2) is valid and the mode frequencies and densities correspond those of the Bogoliubov-de Gennes equations (4,5). It follows that the expectation value of any operator will exhibit beats between the various modes. Since a simple rotation does not induce centre-of-mass (dipole) motion, the lowest-order distortion will arise in the quadrupole moments:

$$Q_{ij}^q(t) \equiv \int \psi^*(\mathbf{x}, t) x_i x_j \psi(\mathbf{x}, t) d\mathbf{x} \quad (28)$$

where $\psi(\mathbf{x}, t)$ is the solution of equation (27). The condensate quadrupole moments in the vertical and horizontal planes will give information on the vortex bending and twisting, respectively. We present results for the scaled moments: $\langle yz \rangle \equiv (2/N_0)Q_{yz}(t)$, in figure (3), and $\langle xy \rangle \equiv (2/N_0)Q_{xy}(t)$, in figure (5), and the corresponding power spectral densities:

$$P_{ij}(\omega) \equiv \left| \int_0^T e^{-i\omega t} Q_{ij}(t) dt \right|^2 \quad (29)$$

in figures (4) and (6), respectively.

3.3. Coherent hydrodynamic states

The hydrostatic spectrum, equation (11), also follows from a simplified version of the the Bogoliubov-de Gennes equations [19] when quantum pressure has been neglected:

$$q^2 [-\nabla^2 + q^{-1}(\nabla^2 q)] h_j^+ - \frac{1}{2}\omega_j^2 h_j^+ = 0 \quad (30)$$

$$[-\nabla^2 + q^{-1}(\nabla^2 q)] (q^2 h_j^-) - \frac{1}{2}\omega_j^2 h_j^- = 0 \quad (31)$$

where $h_j^\pm = u_j \pm v_j$, and q^2 is the vortex-free hydrostatic density given by

$$q^2(x, y, z) = \begin{cases} \left[\mu - \frac{1}{4}(x^2 + y^2 + \lambda^2 z^2) \right] & \text{if } \mu - \frac{1}{4}(x^2 + y^2 + \lambda^2 z^2) \geq 0 \\ 0 & \text{if } \mu - \frac{1}{4}(x^2 + y^2 + \lambda^2 z^2) < 0 \end{cases} \quad (32)$$

These equations can be solved in closed analytic form using series expansions [19] to yield expressions for the quasiparticle amplitudes. The scissors mode quadrupole ($\kappa = 0, m = \pm 1$) for $\lambda > 1$, with $\bar{\rho}^{(h)}(\mathbf{x}) \propto xz$, first proposed by Guéry-Odelin and Stringari [20] and experimentally observed by Maragó et al. [15] has the frequency:

$$\Omega_s = \sqrt{1 + \lambda^2}. \quad (33)$$

Quadrupoles corresponding to $\kappa = 0, m = \pm 2$ are degenerate with frequency: $\Omega_{xy} = \sqrt{2}$.

The scissors mode, selected by sudden rotation θ_0 , introduces a perturbation:

$$V' \approx m_a \omega_0^2 \theta_0 (1 - \lambda^2) xz \quad (34)$$

In the absence of a vortex ($\kappa = 0$), coupling to the degenerate $m = \pm 1$ states is equal and opposite, and no helicity arises. If a vortex is present ($\kappa = 1$), the coupling is asymmetric since the state $m = +|m|$ rotates with the condensate flow at frequency ω^+ , whereas the mode $m = -|m|$ is counter-rotating at frequency ω^- , see figure 1. The frequency difference was calculated analytically using a hydrodynamic model [22] with the result that

$$\omega^+ - \omega^- = \frac{2\langle L_z \rangle}{m_a \langle r^2 + 2z^2 \rangle} = \frac{\langle L_z \rangle}{I_{xx}} = \frac{\langle L_z \rangle}{I_{yy}} \quad (35)$$

Table 1. Table of mode excitation frequencies for $\lambda = \sqrt{7}$ as a function of the interaction strength: $C = 8\pi N_0 a_s (\hbar/2m_a \omega_0)^{-\frac{1}{2}}$. The full spectrum is shown in figure 7. The selected modes in the table are are: (1) $(h; 0, 1, 1)$; (3) $(h; 0, -1, 1)$; (c) $(h; 0, 2, 0)$; and (d) $(h; 0, -2, 0)$. The first entry in each column is the result from the Bogoliubov-de Gennes equations (3–5). The numbers in brackets correspond to the time-dependent linear response method of calculation. The Bogoliubov-de Gennes results for the frequency of precession are denoted by ω_p . All angular frequencies are in units of ω_0 .

C	ω_p	(1)		(3)		(c)		(d)	
0	0.000	3.646	(3.646)	1.646	(1.645)	2.000	(2.001)	0.000	(0.000)
50	0.075	3.488	(3.495)	1.625	(1.627)	1.946	(1.896)	0.522	(0.516)
100	0.110	3.401	(3.398)	1.590	(1.591)	1.889	(1.846)	0.738	(0.730)
250	0.145	3.267	(3.257)	1.483	(1.491)	1.787	(1.780)	0.984	(1.016)
500	0.149	3.169	(3.165)	1.354	(1.370)	1.708	(1.744)	0.111	(1.105)
1000	0.137	3.085	(3.079)	1.201	(1.194)	1.640	(1.644)	1.197	(1.195)

where I_{xx} is the principal inertia moment about a horizontal axis. The result also agrees with the result of Svidzinsky and Fetter [11] which treats the vortex core as a perturbation of the hydrostatic Thomas-Fermi density. The same result can be found and understood using a classical model of the motion (section 3.4).

To obtain the amplitude of precession and nutation, the populations of the excited modes are required. Since the tilting is small and sudden, we can use diabatic perturbation theory. A small sudden rotation by an angle θ_0 about the y -axis, with generator $L_y = (2i)^{-1}(L_+ - L_-)$, gives rise to the function:

$$\psi_h(t=0) \approx \exp[-i\hbar^{-1}\theta_0 L_y] \phi_h \quad (36)$$

The amplitudes are found by projection to the modes in the rotated frame of reference. From equation (2):

$$\psi_h(\mathbf{x}, t) e^{i\mu t} \approx \sqrt{N_0} \phi_h(\mathbf{x}, t) + \sum_j [a_j(t) u_j(\mathbf{x}) e^{-i\omega_j t} + a_j^*(t) v_j^*(\mathbf{x}) e^{+i\omega_j t}]$$

and the coefficients $a_j(t)$ will be time-independent. Projection by the hydrodynamic state $h_j^- \equiv u_j - v_j$ gives the time-independent amplitudes a_j

$$(h_j^-, h_j^+) a_j \approx (h_j^-, \exp[-\frac{1}{2}\hbar^{-1}\theta_0(L_+ - L_-)] \phi_h) \quad (37)$$

The rotation mixes the initial state with $m = \pm 1, \pm 2$, to order θ_0 , and θ_0^2 , respectively. We have overlooked the density distortion of the vortex, though included the angular momentum. Since the vortex core distorts the density over a comparatively small volume of the condensate, then to a first approximation the density is the axisymmetric Thomas-Fermi distribution, equation (32). Therefore, as a simple first-order approximation we take

$$\phi_h = C^{-\frac{1}{2}} q(r, z) e^{i\kappa\varphi}$$

where q^2 is given by equation (32). The time-independent equations (30,31) can be used to calculate the quasiparticle functions, and the transition amplitudes, a_j given by (37), can be extracted analytically as shown in [21]. In this approximation, the excitation spectrum is the

same as the vortex free case, and does not include the degeneracy splitting arising in higher-order perturbation theory [22, 11]. The quadrupole excitations in the vertical and horizontal plane are defined as:

$$Q_{yz}^h(t) \equiv \int \psi_h^*(\mathbf{x}, t) yz \psi_h(\mathbf{x}, t) d\mathbf{x} \quad (38)$$

$$Q_{xy}^h(t) \equiv \int \psi_h^*(\mathbf{x}, t) xy \psi_h(\mathbf{x}, t) d\mathbf{x} \quad (39)$$

and can be calculated analytically. The results for this coherent hydrodynamic model are presented in figures 3 and 4.

3.4. Classical model

We use the convention of Goldstein [14] for the Euler angles (ϕ, θ, ψ) , describing the orientation of a set of rotating axes (x', y', z') with respect to a space fixed frame (figure 1). The principal moments of inertia of the vortex-free density, equation (32), are:

$$I_{xx} = \frac{(\lambda^2 + 1)}{3\lambda^2} I_s \quad \text{and} \quad I_{zz} = \frac{2}{3} I_s \quad \text{where} \quad I_s = \frac{3}{7} m_a N_0 \left[\frac{15\lambda N_0 g}{4\pi m_a \omega_0^2} \right]^{\frac{2}{5}} \quad (40)$$

In general the Lagrangian density, \mathcal{L}_a , is given by [23]:

$$\mathcal{L}_a(\rho, \phi_v, \dot{\rho}, \nabla \phi_v, \nabla \rho; \mathbf{x}; t) = \phi_v \dot{\rho} - \frac{1}{2} \rho (\nabla \phi_v)^2 - \rho U - \frac{\hbar^2}{8m_a^2 \rho} (\nabla \rho)^2 \quad (41)$$

where the potential per unit mass is $U = (V_{\text{ext}}/m_a) + (g\rho/2m_a^2)$ and $\mathbf{v} = \nabla \phi_v$. Discarding the last term gives the classical interacting fluid [24] with the corresponding Hamiltonian density:

$$\mathcal{H}_c = \frac{1}{2} \rho \mathbf{v}^2 + \frac{g\rho}{2m_a^2} + \frac{1}{2} \rho \omega_0^2 (x^2 + y^2 + \lambda^2 z^2) \quad (42)$$

At equilibrium the condensate has a hydrostatic (vortex-free) density and angular momentum $N_0 \hbar \kappa$. A small change of orientation of the trap $(\delta\theta)$ creates density and velocity changes, $\tilde{\rho}, \tilde{\mathbf{v}}$:

$$\partial_t \tilde{\rho} + (g/m_a) \nabla \tilde{\rho} = 0 \quad , \quad \partial_t \rho + \nabla \cdot (\rho_0 \nabla \tilde{\mathbf{v}}) = 0 \quad (43)$$

In the body-fixed frame, and for quadrupole (xz) perturbations only, this leads to an effective potential

$$\delta V(\theta) = \frac{1}{2} \omega_0^2 (1 + \lambda^2) \rho_0 (x^2 + z^2) (\delta\theta)^2 \quad (44)$$

Then the Lagrangian in the space-fixed frame has the form, for small θ :

$$L(\theta, \dot{\varphi}, \dot{\theta}, \dot{\psi}, t) = \frac{1}{2} I_{xx} \sin^2 \theta \dot{\psi}^2 + \frac{1}{2} I_{xx} \dot{\theta}^2 + \frac{1}{2} I_{zz} (\dot{\psi} + \dot{\varphi} \cos \theta)^2 - \frac{1}{2} I_{xx} \Omega_s^2 \theta^2 \quad (45)$$

From this Lagrangian, Hamilton's equations are

$$\dot{\varphi} = \frac{(p_\varphi - p_\psi \cos \theta)}{I_{xx} \sin^2 \theta} \quad \dot{\theta} = \frac{p_\theta}{I_{xx}} \quad (46)$$

$$\dot{\psi} = \frac{p_\psi}{I_{zz}} - \frac{(p_\varphi - p_\psi \cos \theta) \cos \theta}{I_{xx} \sin^2 \theta} \quad \dot{p}_\varphi = 0 \quad (47)$$

$$\dot{p}_\theta = \frac{(p_\varphi - p_\psi \cos \theta)(p_\varphi \cos \theta - p_\psi)}{I_{xx} \sin^3 \theta} - I_{xx} \Omega_s^2 \theta \quad \dot{p}_\psi = 0 \quad (48)$$

In anticipation of the numerical results, consider possible analytic solutions of the equations for very small angular displacements θ . The top is aligned vertically ($\theta = 0$) and spinning with angular momentum J_0 , thus $p_\psi = J_0$ and $p_\theta = 0$. The possible singularity at $\theta = 0$ in the equation for $\dot{\varphi}$ can be avoided if $p_\varphi - p_\psi \cos \theta \rightarrow 0$ as $\theta \rightarrow 0$. A steady azimuthal precessional, $\ddot{\varphi} = 0$, independent of $\theta(t)$, arises from the case $p_\psi = p_\varphi = J_0$ in which case, for $\cos \theta \approx 1 - \frac{1}{2}\theta^2$, we have:

$$\dot{\varphi} \approx \frac{J_0}{2I_{xx}}$$

Under the same approximations, and the fact that $\dot{\theta} = p_\theta/I_{xx}$:

$$\dot{p}_\theta \approx - \left(\frac{J_0^2}{I_{xx}} + I_{xx}\Omega_s^2 \right) \theta \quad \ddot{\theta} = - \left(\frac{J_0^2}{I_{xx}^2} + \Omega_s^2 \right) \theta$$

Therefore the vortex motion is described by

$$\theta \approx \theta_0 \sin \sqrt{\Omega_s^2 + (J_0/I_{xx})^2} \cdot t \quad \varphi \approx \frac{J_0}{2I_{xx}} t \quad (49)$$

which describes a steady azimuthal precession, frequency $\omega_p = J_0/2I_{xx}$, combined with sinusoidal nutation at a frequency slightly higher than the vortex-free scissors oscillation. The precessional motion splits the frequencies. It is equivalent to a steady background rotation of the condensate. In analogy to a Doppler shift, internal flow around the z -axis associated with the quantum number $\pm m$ would be shifted so that $\omega^+ - \omega^- \equiv 2\omega_p = J_0/I_{xx}$. This splitting, understood in terms of classical precessional motion, is identical to the quantum expression [11, 22].

Initially the condensate has a pure rotation about the z' -axis so that $\psi = J_0/I_3$, and the condensate is impulsively tilted by an angle θ_0 . The Hamilton equations are solved numerically, with the initial conditions, $t = 0$:

$$\theta = \theta_0 \quad \varphi = 0 \quad (50)$$

$$\psi = 0 \quad p_\varphi = J_0 \cos \theta_0$$

$$p_\theta = 0 \quad p_\psi = J_0$$

The time dependence of the products of inertia is governed by the orientation of the axis of the top and thus will oscillate in time. The transformations between the laboratory and fixed-frame quadrupole gives

$$Q_{xz}^c(t) \equiv \frac{1}{2}(I_{xx} - I_{zz}) \sin 2\theta \cos \varphi \quad (51)$$

$$Q_{yz}^c(t) \equiv \frac{1}{2}(I_{xx} - I_{zz}) \sin 2\theta \sin \varphi \quad (52)$$

$$Q_{xy}^c(t) \equiv \frac{1}{2}(I_{xx} - I_{zz}) \sin 2\varphi \sin^2 \theta \quad (53)$$

Since the inertia moments, I_{xx} and I_{zz} , are constant, the time dependence is entirely governed by $\phi(t)$ and $\theta(t)$. These functions are determined by numerical integration of equations (48) with initial conditions (51). The physical meaning of the quadrupole is clear if one visualises a rigid vortex motion which nutates and precesses. At the instant the vortex is aligned along the $y = 0$ plane, then $\langle yz \rangle = 0$. This happens twice each precession cycle. During the slow precession, the vortex line nutates rapidly between the 1st and 2nd quadrants of the yz -plane

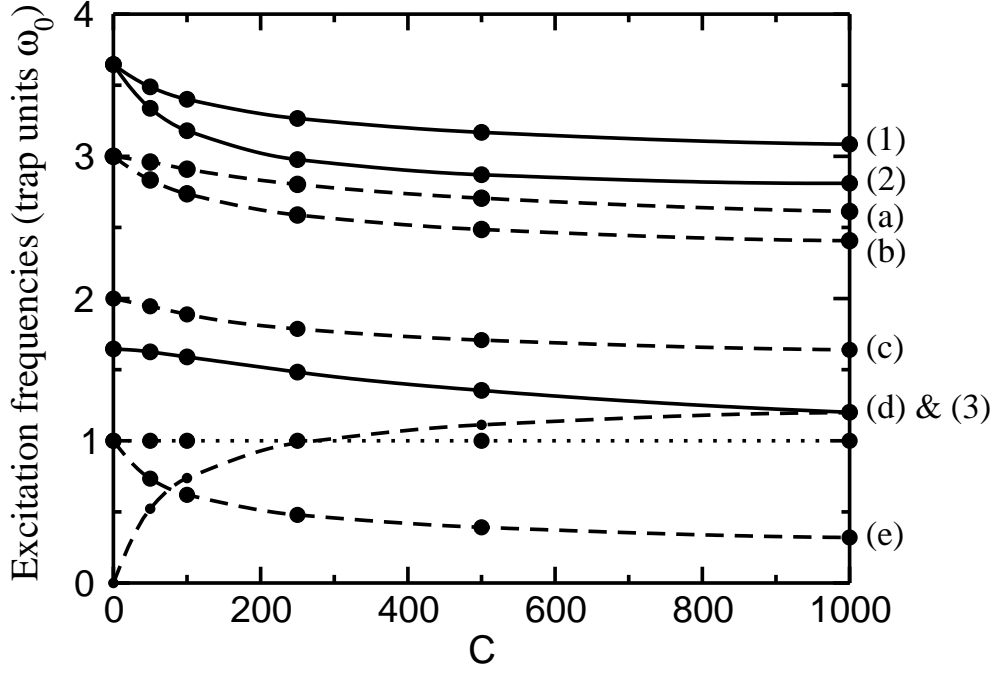


Figure 7. The excitation spectrum of the vortex condensate as a function of interaction strength $C = 8\pi N_0 a_s (\hbar/2m_a \omega_0)^{-\frac{1}{2}}$. The solid lines labelled (1), (2) and (3) correspond to those found in the power spectrum of $\langle yz \rangle$. The dashed lines (a),(b), (c) and (d) are prominent in the quadrupole $\langle xy \rangle$. The centre-of-mass dipole mode (dotted line) is included for completeness as well as the negative frequency mode $(\hbar; 0, -1, 0)$; line (e). The limit $C \rightarrow 0$ corresponds to the ideal gas modes $(i; n_r, n_\theta, n_z)$ with frequencies given by equation (16). Values of selected mode frequencies are given in table 1.

which leads to a change of sign in Q_{xz} each half-cycle of the scissors period. The amplitude of the vertical plane (yz) quadrupole is more easily observable by experiment [13] since it is of order θ_0 (figure 3). The horizontal plane motion, on the other hand, is proportional to θ_0^2 (figure 5).

4. Results and Discussion

4.1. Excitation modes and spectrum

Our numerical studies focus on a singly-quantised vortex ($\kappa = 1$) condensate in a pancake shaped trap $\lambda = \sqrt{7}$, for detailed theoretical discussion, and $\lambda = \sqrt{8} \approx 2.83$ for comparison with experiment. The frequencies of the quadrupole moments can be obtained from the excitation spectrum of the normal modes of the system. The spectra obtained for $\kappa = 1$ and $0 < C < 1000$ are shown in figure 7, and given in table 1. For $C \gg 1000$ the variation in excitation spectrum is slow and smooth, and tends towards asymptotic limits. Consider $C = 1000$ with an equivalent chemical potential for the hydrostatic density in the absence of a vortex: $\mu_{\text{TF}} = (15\lambda C/64\pi)^{\frac{2}{5}} \approx 8.282 \gg 1$. While this lies well within the region of validity of the hydrodynamic approximation, in the sense that $\mu \gg \omega_0$, the trap energy and vortex core inhomogeneity are still significant and one would expect quantal deviations from

the hydrodynamic model. Prior to analysing the motion in detail, an example of the density fluctuations produced by our simulations is shown in figure 2. The time-dependent Gross-Pitaevskii equation (27) is solved in imaginary time with $\kappa = 1$ to generate the initial state of the condensate. The trap is then suddenly tilted by a small angle, $\theta = 10^\circ$, about the y axis and the evolution of the condensate follows the time-dependent Gross-Pitaevskii equation. Surfaces of constant density of the condensate are shown in figure 2 in the tilted space-fixed frame of reference. A vertical cut through the surface reveals the vortex core structure over a single trap period. The first image $t = 0$ is the initial configuration, the subsequent images are taken at regular intervals, $t = 1.3, 2.6, 3.9, 5.2$ and $t = 6.5$, respectively, in units of ω_0^{-1} . The scissors oscillation of the condensate corresponds to nutation, that is quadrupole oscillation in the vertical plane. This creates flow past the vortex producing a Magnus force which results in precession. However when combined with the inhomogeneity in the condensate, the force gives rise to vortex bending and twisting into helical modes of oscillation. The modes of oscillation can be most clearly identified by spectral resolution of the mass moments. A detailed frequency spectrum of the principal modes for gyroscopic excitation is shown in figure 7 as a function of interaction strength C .

4.2. Vortex precession

Consider firstly the scissors $\langle yz \rangle$ or $\langle xz \rangle$ mode of oscillation; the quadrupole moment results are presented in figure 3 and the corresponding frequency spectrum in figure 4. Data obtained using the direct solution of the time-dependent Gross-Pitaevskii equation are compared with the coherent hydrodynamic calculation, and the classical top results. The parameters $C = 1000$ and $\lambda = \sqrt{7}$ with N_0 atoms and $\theta_0 = 4^\circ$ translate to : $I_s = (6/7)\mu_{\text{TF}}N_0$, $I_{xx} = (16/49)\mu_{\text{TF}}N_0$ and $I_{zz} = (4/7)\mu_{\text{TF}}N_0$. Considered as a classical rigid top, the condensate, viewed along the x -direction will exhibit quadrupole oscillations due to nutation. If the top precesses then this moment vanishes each time the axis nutates along the xz -plane. Using equation (53), the classical moment $\langle yz \rangle$ oscillates with a carrier frequency $\omega_p = (49/32)\mu_{\text{TF}}^{-1} \approx 0.185\omega_0$, and carrier amplitude $\langle yz \rangle_{\text{max}} = 2(I_{zz} - I_{xx})\theta_0 \approx 0.283$. The classical prediction for the beat period of the $\langle yz \rangle$ quadrupole, is in fairly good agreement with the unperturbed coherent hydrodynamic results $\omega_p = \frac{1}{2}(3 - \sqrt{7})\omega_0 \approx 0.177\omega_0$ as shown in figure 3. Neither of these results compare well with the more accurate lower-frequency result from the Gross-Pitaevskii equation: $\omega_p = 0.137\omega_0$. The lower beat (precession) frequency (figure 3) contrasts with higher mode frequencies compared with the hydrodynamic limit, as illustrated in figure 4. In figure 7 it is clear that, for $C = 1000$, the curves (1) and (2) corresponding to these modes have not reached the asymptotic limit $C \rightarrow \infty$.

Very recently measurements of vortex precession [13] in a trap were made under the following conditions $\lambda \approx 2.83$, $\omega_0 = 2\pi \times 62$ Hz, and $N_0 \approx 19000 \pm 4000$ atoms. This corresponds to an interaction strength $C \approx 2870 \pm 600$ which is within the hydrodynamic regime but should exhibit quantal effects. The classical precession frequency is $\omega_p^c = 0.120 \pm 0.012\omega_0$ where the error is due to the uncertainty in N_0 . A calculation using the Gross-Pitaevskii equation gives $\omega_p^{\text{GPE}} \approx 0.104 \pm 0.08\omega_0$. As in the case previously discussed

($\lambda = \sqrt{7}$, $C = 1000$) this rate of precession is slightly lower than the classical/hydrodynamic prediction. The equivalent frequencies for the vortex precession are $f_p^{\text{GPE}} \approx 6.5 \pm 0.5\text{Hz}$ and $f_p^c \approx 7.4 \pm 0.5\text{Hz}$. Measurements were performed by imaging the vortex line in the horizontal plane and trap tilting along both the xz and yz planes and were in good agreement. Taking the average of the results gives the experimental estimate $f^{\text{exp}} = 7.8 \pm 0.6\text{Hz}$; a slightly faster rate of precession than the quantal prediction, and more in line with hydrodynamic theory.

While the limitations of zero temperature models, as described in this paper, are well known, the hydrodynamic approximation is generally less accurate than the Gross-Pitaevskii equation. Moreover, important effects neglected by this model are the viscous effects of the thermal fluid, as observed [13]. However, these effects would probably reduce ω_p^{GPE} further and thus increase the gap between experiment and theory. It has been suggested [13] that two other effects might have a role in explaining the differences. Firstly, the possibility of off-centre precession [25] and secondly, the influence of additional edge vortices [26] might have significant effects. While the results of the observations and the theory outlined above are in very good agreement, there is a considerable margin for improving the simulations to study the contribution of these effects and of the influence of thermal damping.

Considering some of the other modes, we note that this scissors excitation of the vortex state weakly populates a low-frequency mode at $\omega = 1.201$; on figure 4 and labelled line (3), and also marked on figure 7. This is the lowest z -dipole mode $(i; 0, 0, 1)/(h; 0, -1, 1)$. The variation of frequency of the mode is given in table 1 and drawn in figure 7. Checks on the numerical accuracy of the numerical methods were also provided by studying the centre-of-mass modes whose frequencies remains constant as the particle number or interaction strength C varies; a consequence of the Kohn theorem [27, 28], figure 7. We note the labelling of axial excitation modes $(i; 0, 2, 1) \rightarrow (h; 0, +1, 1)$ and $(i; 1, 0, 1) \rightarrow (h; 1, -1, 1)$, reflects the quadrupole symmetry in the hydrodynamic regime. Values of the $(h; 0, +1, 1)$ mode frequency are given in table 1, in which the highly accurate Bogoliubov de-Gennes results are compared with results using the time-dependent linear response method [18]. This confirms the accuracy both of the direct time-dependent method and the linear response approximation.

4.3. Kelvin modes

Kelvin modes are self-induced helical waves of a vortex line and have a well-established dispersion relation for infinite homogeneous fluids [29]. However, in a trapped condensate, the finite boundaries means these modes are quantised, and the inhomogeneity of the condensate means that the fluid pressure varies along the vortex line. The signature of the Kelvin modes is the distortion of the vortex line and can be detected in the gyroscope motion. The lowest-order and most strongly-coupled modes, $m = \pm 1$, are excited by the small angle rotation of the trap. Since the modes $m = +1$ and $m = -1$ are populated in approximately equal weights this leads to a kink in the vortex in the vertical plane. The bending and twisting of the vortex line is more pronounced at the low-density low-pressure edges of the condensate (figure 2). Analysis of the horizontal plane quadrupole moment $\langle xy \rangle$ shows periodicity but irregularity (figure 5). The two-mode classical theory, equation (53), strongly disagrees with

the quantal results shown in figure (5). The amplitude of oscillation is much larger than classically predicted, and is associated with the vortex s -shape outward bend. However the main feature is the quantal oscillations that indicate twisting, that is bending of the vortex projected onto the $\langle xy \rangle$ plane. The horizontal-plane spectrum (figure 6) is dominated by two pairs of lines labelled (a,b) and (c,d). Figure 7 and table 1 indicate the frequency variation, with atom number C , of the helical modes. The lines (c) and (d) are the quadrupole pair $(h; 1, +2, 0)$ and $(h; 1, -2, 0)$, respectively. In the hydrodynamic limit with $\kappa = 0$ they corresponds to the doubly-degenerate xy -quadrupole with frequency, $\omega = \sqrt{2}$.

The correlation of the pair (c) and (d) to the ideal gas states $(i; 1, 3, 0)$ and $(i; 1, -1, 0)$, is shown in figure 6. The splitting of this quadrupole pair $\Delta\omega = 0.443\omega_0$ is a signature of vortex precession, though again it is substantially smaller than the classical prediction $4\omega_p \approx 0.548$ associated with a rigid vortex crossing the $x = 0$ and $y = 0$ planes during precession. The dominance of mode (c) over (d) is apparent (figure 6) and means the vortex has a positive helicity of $m = +2$. Indeed, the strong coupling of $m = 2$ states with vortex motion has been used to measure the angular momentum of the vortex state [26]. The pair of high-frequency lines (a) and (b) also contribute strongly to the spectrum. These are the dipole-like modes $(h; 1, 1, 0)$ and $(h; 2, -1, 0)$, degenerate as $C \rightarrow 0$ with symmetry $(i; 1, 2, 0)$ and $(i; 2, 0, 0)$. The pair of lines are of approximately equal weighting and therefore cancel helicities. As $C \rightarrow \infty$, these lines converge slowly towards the common limit $\omega = 2.321$. Finally the spectrum shows two low-intensity lines at $\omega \approx 0.274$ and $\omega \approx 1.892$. These are not new modes but rather vestiges of the $\langle yz \rangle$ modes; the low frequency line being the beat frequency corresponding to the splitting of lines (1) and (2) in figure 4, and the higher frequency line, the frequency difference of modes (1) and (3).

5. Conclusions

In conclusion, we have studied the gyroscopic dynamics of a trapped Bose-Einstein condensate containing a vortex. We modelled the system using a classical top description and numerically by solution of the time-dependent Gross-Pitaevskii equation. We also compared our results with the hydrodynamic approximation. The linear-response equations for the system were solved giving the excitation spectra and amplitudes. The superfluid precession and nutation of the vortex were found to display quantum frequency shifts. The precession frequency was calculated and found to be consistent with recent experiments, though a small discrepancy exists. Vortex bending and twisting modes of excitation were observed. We found, in the scissors excitation of the vortex state, that vortex bending in the vertical plane is associated with the $m = \pm 1$ modes of oscillation, while the helical oscillation, vortex twisting, is dominated by the $m = +2$ Kelvin mode.

We are very grateful to Profs. C. J. Foot (Oxford) and J.-P. Hansen (Bergen) for many helpful discussions and exchanges on this problem. We gratefully acknowledge the support of the Bergen Computational Physics Laboratory in the framework of the European Community - Access to Research Infrastructure action of the Improving Human Potential Programme; Dermot McPeake thanks the Department for Employment and Learning Northern Ireland for

financial support through the provision of a Postgraduate Studentship. Halvor Møll Nilsen acknowledges support from the Norwegian Research Council.

References

- [1] Anderson M H *et al* 1995 *Science* **269**, 198
- [2] Matthews M R *et al* 1999 *Phys. Rev. Lett* **83** 2502
- [3] Madison K W , Chevy F, Wohlleben W and Dalibard J 2000 *Phys. Rev. Lett* **84** 806 .
- [4] Abo-Shaer J R, Raman C, Vogels J M and Ketterle W 2001 *Science* **92** 476
- [5] Zambelli F and Stringari S 2001 *Phys. Rev. A* **63** 033602
- [6] Maragó O *et al* 2002 *J. Phys.: Condensed matter* **14** 343
- [7] Pines D and Nozières P 1965 *Quantum Fluids* (Addison Wesley)
- [8] Winiecki T, Jackson B, McCann J F and Adams C S 2000 *J. Phys. B* **19** 4069
- [9] Winiecki T, McCann J F and Adams C S 1999 *Phys. Rev. Lett.* **82** 5186
- [10] Raman C *et al* 1999 *Phys. Rev. Lett* **83** 2502
- [11] Svidzinsky A and Fetter A L 1998 *Phys. Rev. A* **58** 3168
- [12] Stringari S 2001 *Phys. Rev. Lett* **86** 4725
- [13] Hodby E, Hopkins S A, Hechenblaikner G, Smith N L and Foot C J 2002 cond-mat/0209634
- [14] Goldstein H 1980 *Classical Mechanics* (Addison Wesley)
- [15] Maragó O M, Hopkins S A, Arlt J, Hodby E, Hechenblaikner G and Foot C J 2000 *Phys. Rev. Lett.* **84** 2056
- [16] Hodby E *et al* 2001 *Phys. Rev. Lett* **86** 2196
- [17] Maragó O *et al* 2001 *Phys. Rev. Lett* **86** 3938
- [18] McPeake D, Nilsen H M and McCann J F 2002 *Phys. Rev. A* **65** 063601
- [19] Öhberg P, Surkov E L, Tottonen I, Stenholm S, Wilkens M and Shlyapnikov G V 1997 *Phys. Rev. A* **56** 3346
- [20] Guéry-Odelin D and Stringari S 1999 *Phys. Rev. Lett* **83** 4452
- [21] Nilsen H M 2003 *in preparation*
- [22] Zambelli F and Stringari S 1998 *Phys. Rev. Lett* **81** 1754
- [23] Negele J W and Orland H 1988 *Quantum Many-Particle Systems* (Addison Wesley)
- [24] Oden J T and Reddy J N 1976 *Variational methods in Theoretical Mechanics* (Springer-Verlag)
- [25] Jackson B, McCann J F and Adams C S 2000 *Phys. Rev. A* **61** 013604
- [26] Chevy F, Madison K W and Dalibard J 2000 *Phys. Rev. Lett* **85** 2223
- [27] Hutchinson D A W, Zaremba E and Griffin A 1996 *Phys. Rev. Lett* **78** 1842
- [28] Jobson J F 1994 *Phys. Rev. Lett.* **73** 2244
- [29] Donnelly R J 1991 *Quantized Vortices in Helium II* (CUP).

